

Effect of phantom dark energy on the holographic thermalization

Xiao-Xiong Zeng¹, Xin-Yun Hu¹, Li-Fang Li (corresponding author)^{a,2}

¹ School of Science, Chongqing Jiaotong University, Chongqing, 400074, China

²State Key Laboratory of Space Weather, Center for Space Science and Applied Research, Chinese Academy of Sciences, Beijing, 100190, China

the date of receipt and acceptance should be inserted later

Abstract Gravitational collapse of a shell of charged dust surrounded by the phantom dark energy is probed by the minimal area surface, which is dual to probe the thermalization in the boundary quantum field by expectation values of Wilson loop in the framework of the AdS/CFT correspondence. We investigated mainly the effect of the phantom dark energy parameter and chemical potential on the thermalization. The result shows that the smaller the phantom dark energy parameter is, the easier the plasma thermalizes as the chemical potential is fixed, and the larger the chemical potential is, the harder the plasma thermalizes as the dark energy parameter is fixed. We get the fitting function of the thermalization curve and with it, the thermalization velocity and thermalization acceleration are discussed.

Keywords Holographic thermalization, phantom dark energy, non-equilibrium

1 Introduction

Recent years, more and more theoretical physicists have paid their attention on the applications of the AdS/CFT correspondence[1]. It can not only check the effectiveness of this correspondence indirectly, but also provide a method to deal with some problems in strongly coupled system[2,3,4,5,6,7]. One of the strongly coupled systems is the quark gluon plasma which are produced in heavy ion colliders such as the RHIC and LHC. The properties of the quark gluon plasma have been investigated extensively and we know that it behaves as an ideal fluid with a very small shear viscosity over entropy density ratio[8]. But the process of formation of quark gluon plasma after a heavy ion collision, often referred

to as thermalization, is not well understood until now. Recently some physicists have devoted themselves to addressing this problem from the viewpoint of holography, which is called holographic thermalization. The most prominent property for the thermalization is that it is a non-equilibrium process. From the AdS/CFT correspondence, we know that the initial state before the thermalization is dual to a pure AdS, and the last state after the thermalization is dual to a stationary black hole. Therefore, to describe the thermalization process, one should construct a dynamical background in the bulk, which can be described as black hole formation or black hole merger.

Now, there have been many models to study this far-from-equilibrium thermalization behaviors[9,10,11,12,13,14,15,16,17]. A slightly different and simpler model on this topic was put forward by Balasubramanian et al.[18,19], where the dynamical background was treated as the gravitational collapse of a shell of dust. They claimed that the thermalization process can be probed by the equal-time two-point correlation functions of local gauge invariant operators, expectation values of Wilson loop operators, and entanglement entropy, which in the gravity side correspond to minimal lengths, areas, and volumes in AdS space, respectively. An important conclusion from their model is that the thermalization time is closer to the experiment data produced in RHIC and LHC. In addition, they found that the thermalization is a top-down process, in contrast to the predictions of bottom-up thermalization from perturbative approaches[20], and there is a slight delay in the onset of thermalization. Now such model has been generalized to the bulk geometry with electrostatic potential [21,22,23], high curvature corrections [24,25,26,27], and some other gravity models [28,29,30,31,32,33,34,35,36,37,38,39,40,41,42,43,44].

^ae-mail: lilf@itp.ac.cn

In this paper, we intend to study holographic thermalization in the bulk surrounded by phantom dark energy. The phantom dark energy is the scalar field with a negative kinetic term with an equation of state parameter $\omega < -1$. As already known, the presence of cosmological phantom fields continues to receive supports from both collected observational data [45] and theoretical models [46]. All these programs have pointed out an accelerated expansion of the universe, dominated by an exotic fluid of negative pressure. Furthermore, there are evidences suggesting the exotic fluid could be of phantom nature [47, 48]. Since then, an interest in phantom fields has grown and resulted in many phantom black hole solutions [49, 52]. In recent years, many issues pertaining to phantom black hole, such as thermodynamic stability [53] and light paths [54, 55] have been dealt with. In this paper, we study holographic thermalization in the spacetime dominated by phantom dark energy. The authors in ref. [44] has studied the holographic thermalization dominated by quintessence dark energy and their results show that the smaller the state parameter of quintessence is, the harder the plasma to thermalize. Considering the first year WMAP data together with the 2dF galaxy survey and the supernova Ia data favor the phantom energy over the cosmological constant and the quintessence, here we study the effect of phantom dark energy on the holographic thermalization. Our results show that the state parameters of dark energy play different roles in the process of holographic thermalization. Our results here shows that the smaller the phantom dark energy parameter is, the easier the plasma to thermalize when the chemical potential is fixed, which is different from the case produced by quintessence dark energy.

The structure of this paper is outlined as follows. In Section 2, we will briefly review the gravitational collapse solution in the spacetime dominated by the phantom dark energy. In Section 3, we derive the equations of motion of the minimal area surface theoretically firstly, and then perform a systematic analysis about how the dark energy parameters and chemical potential affect the thermalization time resorting to numerical calculation. We also study the thermalization velocity and thermalization acceleration with the fitting functions of the thermalization probes. The last section is devoted to discussions and conclusions.

2 Gravitational collapse surrounded by phantom dark energy

Start from the action

$$S = \int d^4x \sqrt{-g} [R + 2\eta F^{\mu\nu} F_{\mu\nu} + 2\Lambda], \quad (1)$$

reference [56] recently obtained a phantom Reissner-Nordstrom AdS black hole solution

$$ds^2 = -f(r)dt^2 + f^{-1}(r)dr^2 + r^2 d\phi^2 + r^2 \sin^2 \phi d\varphi^2, \quad (2)$$

where

$$f(r) = 1 - \frac{2M}{r} + \eta \frac{q^2}{r^2} + \frac{r^2}{L^2}. \quad (3)$$

In which L is the radius of the AdS black hole, η is the phantom dark energy parameter. For $\eta = 1$, the solution in Eq.(2) represents for the Reissner-Nordstrom-AdS black hole. There is also a purely electric gauge field given by

$$A_t = (u - \frac{q}{r}), \quad (4)$$

where u is a constant corresponding to the electrostatic potential at $r \rightarrow \infty$, which will be related to the chemical potential in the dual gauge theory according to the AdS/CFT correspondence. It is defined such that the gauge field vanishes at the horizon, namely $u = q/r_h$.

In the context of the AdS/CFT correspondence, one is often interested in dual gauge theories living on flat space. In order to achieve this goal, one often use the infinite volume limit [57]. After this step, we can get the phantom Reissner-Nordstrom-AdS black brane solution

$$ds^2 = -F(r)dt^2 + F^{-1}(r)dr^2 + r^2 dx_i^2, \quad (5)$$

in which $i = 1, 2$, and

$$F(r) = -\frac{2M}{r} + \eta \frac{q^2}{r^2} + \frac{r^2}{L^2}. \quad (6)$$

In this case, the event horizon, defined by $F(r_h) = 0$, is plane instead of sphere. According to the definition of the surface gravity, we also can get the Hawking temperature emitting from the black brane

$$T = \frac{\kappa}{2\pi} = \frac{1}{4\pi} \left(\frac{2M}{r_h^2} - \eta \frac{2q^2}{r_h^3} + \frac{2r_h}{L^2} \right), \quad (7)$$

which in the framework of AdS/CFT can be viewed as the equilibrium temperature of the dual field theory living on the boundary.

To get a Vaidya type evolving black brane, we will reexpress the metric in Eq.(5) in Eddington-Finkelstein coordinate $dv = dt + \frac{dr}{F(r)}$, and then rewrite it with the inverse radial coordinate $z = \frac{L^2}{r}$. The background spacetime in Eq.(5) changes into

$$ds^2 = \frac{1}{z^2} [-H(z)dv^2 - 2dz dv + dx_i^2], \quad (8)$$

where L has been set to 1, and

$$H(z) = 1 - 2Mz^3 + \eta q^2 z^4. \quad (9)$$

Treating the mass parameter in Eq.(9) as an arbitrary function of v , Eq.(8) can be regarded as a gravitational collapse solution surrounded by phantom dark energy [18,19,21,22]. This solution is not a solution of the action in Eq.(1) anymore. It includes the contributions of some external matter fields. As one can show, such a metric is sourced by the null dust with the energy momentum tensor flux and gauge flux [21,22]

$$\begin{aligned} 8\pi GT_{\mu\nu}^{matter} &= z^2[\dot{M}(v) - 2zq(v)\dot{q}(v)]\delta_{\mu\nu}\delta_{vv}, \\ 8\pi GJ_{matter}^{\mu} &= z^4\dot{q}(v)\delta^{\mu z}, \end{aligned} \quad (10)$$

where the dot stands for derivative with respect to coordinate v , $M(v)$ and $q(v)$ are the mass and charge of a collapsing black brane

3 Holographic thermalization

In the previous section, we have got a gravitational collapse solution which describes the collapse of a thin-shell of charged dust from the boundary toward the bulk interior of asymptotically anti-de Sitter spaces. According to the AdS/CFT correspondence, this process is dual to the thermalization of plasma of quarks and gluons which are formed in heavy ion colliders such as the RHIC and LHC. To describe the thermalization more comprehensive, we should have an initial state and an equilibrium state, which is dual to a pure AdS and a stationary black brane respectively. Recent investigations show that as the mass $M(v)$ and charge $q(v)$ are written as the smooth functions [18,19,21,22]

$$M(v) = \frac{M}{2} \left(1 + \tanh \frac{v}{v_0} \right), \quad (11)$$

$$q(v) = \frac{q}{2} \left(1 + \tanh \frac{v}{v_0} \right), \quad (12)$$

where v_0 represents a finite shell thickness, one can construct such a gravity model. In this case, in the limit $v \rightarrow -\infty$, the mass vanishes and the background in Eq.(8) corresponds to a pure AdS space. While in the limit $v \rightarrow \infty$, the mass is a constant and the background corresponds to a phantom Reissner-Nordstrom-AdS black brane. Thus for different values of the time v , the background in Eq.(8) stands for different stages of gravitational collapse, which represents for different stages of thermalization in the dual conformal field theory.

3.1 Nonlocal probes

As the gravity model describing the thermalization is constructed, we will choose proper observables to probe

it. Since local observables in the boundary such as expectation values of the energy-momentum tensor are not sensitive to the thermalization process, one needs to consider the non-local observables such as the two-point correlation functions, expectation values of Wilson loops, and entanglement entropy. Recent investigations show that all of them have similar behavior, thus we are interested only in the expectation values of Wilson loops. Wilson loop operator is defined as a path ordered integral of gauge field over a closed contour, and its expectation value is approximated geometrically by the AdS/CFT correspondence as [19,58]

$$\langle W(C) \rangle \approx e^{-\frac{A_{ren}(\Sigma)}{2\pi\alpha'}}, \quad (13)$$

where C is the closed contour, Σ is the minimal bulk surface ending on C with A_{ren} its renormalized minimal area surface, and α' is the Regge slope parameter.

Here we are focusing solely on the rectangular space-like Wilson loop. In this case, the enclosed rectangle can always be chosen to be centered at the coordinate origin and lying on the $x_1 - x_2$ plane with the assumption that the corresponding bulk surface is invariant along the x_2 direction. The area of the minimal area surface is written usually as [59]

$$A = \int \sqrt{g_{\mu\nu} dx^\mu dx^\nu} dx \int dy, \quad (14)$$

here for notational simplicity, x_1 has been replaced by x and x_2 has been replaced by y . For the Vaidya-like AdS black branes in Eq.(8), the area of the minimal area surface can be written as

$$A = \int_{\frac{l}{2}}^{\frac{l}{2}} dx \frac{\sqrt{1 - 2z'(x)v'(x) - H(v,z)v'(x)^2}}{z(x)^2}, \quad (15)$$

where l is the boundary separation along x direction. As to Eq.(15), we can treat the integral as a Lagrangian \mathcal{L} and with it we can get the equations of motion of $z(x)$ and $v(x)$

$$\begin{aligned} 0 &= 4 - 4v'(x)^2 H(v,z) - 8v'(x)z'(x) - 2z(x)v''(x) \\ &\quad + z(x)v'(x)^2 \partial_z H(v,z), \end{aligned} \quad (16)$$

$$\begin{aligned} 0 &= v'(x)z'(x)\partial_z H(v,z) + \frac{1}{2}v'(x)^2 \partial_v H(v,z) \\ &\quad + v''(x)H(v,z) + z''(x). \end{aligned} \quad (17)$$

To solve these equations, we need to consider the symmetry of the minimal area surface and impose the following boundary conditions

$$z(0) = z_*, v(0) = v_*, v'(0) = z'(0) = 0. \quad (18)$$

In addition, the area A is divergent due to its contribution near the AdS boundary. To eliminate it, we should impose a cutoff near the boundary

$$z\left(\frac{l}{2}\right) = z_0, v\left(\frac{l}{2}\right) = t_0, \quad (19)$$

where z_0 is the IR radial cut-off and t_0 is the time that the minimal area surface approaches to the boundary, which is called as the thermalization time usually. AS the divergent part of A is subtracted, the minimal area surface, called renormalized minimal area surface, can be cast into

$$A_{ren} = 2 \int_0^{\frac{1}{2}} dx \frac{z_*^2}{z(x)^4} - \frac{2}{z_0}. \quad (20)$$

Note that here we have used the conserved equations obtained from the Lagrangian \mathcal{L} in Eq.(15), and $\frac{2}{z_0}$ is the contribution of the minimal area surface in the AdS boundary[18,19].

3.2 Numerical results

In this section, we will solve the equations of motion of minimal area surface numerically, and then explore how the chemical potential and phantom dark energy coefficient affect the thermalization. During the numerics, we will take the shell thickness and UV cut-off as $v_0 = 0.01$, $z_0 = 0.01$ respectively.

According to the AdS/CFT correspondence, we know that the electromagnetic field in the bulk is dual to the chemical potential in the dual quantum field theory, therefore we will use the electromagnetic field defined in Eq.(4) to explore the effect of the chemical potential on the thermalization process in the AdS boundary. When we investigate the effect of the chemical potential on the thermalization, the quantity which is physically meaningful is the ratio of u/T , where T is the Hawking temperature of the phantom Reissner-Nordstrom-AdS black brane. However, as stressed in [21,60], the chemical potential has energy units in the dual field theory ($[u] = 1/[L]$) while A_μ defined in Eq.(4) is dimensionless. Thus one has to redefine the electromagnetic field as $\tilde{A}_\mu = A_\mu/p$, where p is a scale with length unit that depends on the particular compactification. Therefore, through this paper we will use the following ratio

$$\frac{u}{T} = \frac{\lim_{r \rightarrow \infty} \tilde{A}_\mu}{T} = \frac{2q(1 + \eta q^2)}{p(3 - \eta q^2)}, \quad (21)$$

to check the effect of the chemical potential on the thermalization time, in which we have set the horizon $r_h = 1$. For simplicity, we will call the ratio in Eq.(21) as chemical potential hereafter. For the phantom dark energy parameter, we know that it satisfies the condition $\eta \leq -1$, in this paper, we will choose $\eta = -1, -2, -3$ in our numerical result. In addition, we know that when $\eta = 1$, the solution in Eq.(2) stands for the Reissner-Nordstrom-AdS black brane. To compare conveniently, we will also study the case $\eta = 1$.

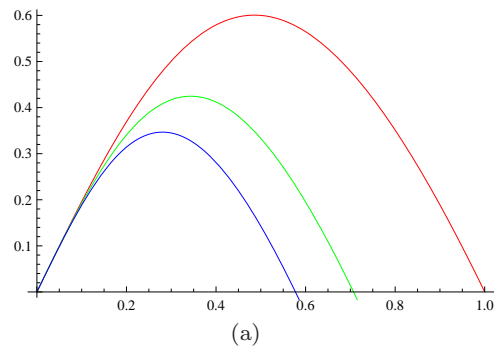


Fig. 1 Change of u/T to the charge q . The red line, green line and blue line correspond to $q = -1, -2, -3$ respectively.

From Eq.(21), we know that for $\eta = 1$, the chemical potential raises from $0 \rightarrow \infty$ provided q changes from 0 to $\sqrt{3}$. While for $\eta \leq -1$, the chemical potential is not monotonous as the charge increases, please see Figure (1). For $\eta = -1, -2, -3$, the chemical potential increases monotonously for $0 < q < 0.49, 0 < q < 0.35, 0 < q < 0.28$ respectively, and monotone decreasing for the other values. To investigate conveniently, we will choose $q = 0.5, 0.7, 0.9$ in this paper. With this choice, from figure (1) we know that for the negative phantom dark energy parameters, as the charge increases, the chemical potential decreases, which is different from the case $\eta = 1$ where the chemical potential increases when the charge increases.

With the initial conditions in Eq.(18), we will solve $z(x)$ and $v(x)$ firstly. When we are interested in the effect of chemical potential on the thermalization, the phantom dark energy coefficient is fixed, and when we are interested in the effect of phantom dark energy coefficient on the thermalization, the chemical potential is fixed. Since different initial time v_* corresponds to different stages of the thermalization, we will study whether the phantom dark energy coefficient and chemical potential have the same effect on the thermalization for different v_* .

The result is listed in Table (1), from it, we can observe the following phenomena:

- For a fixed chemical potential, as the phantom dark energy parameter decreases, the thermalization time increases, which means that the small dark energy parameters delay the thermalization;
- As the charge increases, the thermalization time increases for the positive dark energy parameter while it decreases for the negative parameters. Namely the charge has opposite effect on the thermalization time for the positive and negative parameters. However, as the charge raises, we know that the chemical potential increases for the positive parameter, and decreases for the negative parameters. So we

$v_* = -0.888$	$\eta = 1$	$q = 0.5$ 0.989522	$q = 0.7$ 0.999862	$q = 0.9$ 1.01398
	$\eta = -1$	0.969131	0.9597	0.947474
	$\eta = -2$	0.959202	0.94115	0.918376
	$\eta = -3$	0.949734	0.923542	0.891606
$v_* = -0.555$	$\eta = 1$	1.34905	1.37703	1.41573
	$\eta = -1$	1.29452	1.26975	1.23855
	$\eta = -2$	1.26889	1.22264	1.16637
	$\eta = -3$	1.24432	1.17899	1.10331
$v_* = -0.333$	$\eta = 1$	1.52816	1.56579	1.61914
	$\eta = -1$	1.45507	1.42259	1.38149
	$\eta = -2$	1.42132	1.36125	1.29001
	$\eta = -3$	1.38917	1.30584	1.21261

Table 1 The thermalization time t_0 of the minimal area surface probe for different phantom dark energy coefficient and different charge at $v_* = -0.888, -0.555, -0.333$ respectively.

conclude that for all the phantom dark energy parameter, as the chemical potential raises, the thermalization time increases.

- For different initial thermalization time, the effect of the phantom dark energy parameter and the chemical potential on the thermalization are the same. Thus we can predict that this effect would be the same to the whole thermalization time.

With the numeric result of $z(x)$, we can further get the renormalized minimal area surface defined in Eq.(20). The result is shown in Figure (2) and Figure (3). In Figure (2), we fix the chemical potential to investigate the effect of the phantom dark energy parameter on the thermalization, while in Figure (3) we fix the phantom dark energy parameter to investigate the effect of chemical potential on the thermalization. We are interested in the l independent quantity $\bar{\delta A} \equiv A_{ren}/l$, $\bar{\delta A}_q \equiv A_q/l$, where A_q is the renormalized minimal area surface at the equilibrium state. To observe the thermalization conveniently, we plot the quantity $\bar{\delta A} - \bar{\delta A}_q$. In this case, the thermalized state is labeled by the null point of $\bar{\delta A} - \bar{\delta A}_q$. In each picture, the vertical axis indicates the renormalized minimal area surface while the horizontal axis indicates the thermalization time t_0 .

From Figure (2), we know that as the phantom dark energy parameter decreases, the thermalization time increases. That is, the small phantom dark energy parameter promotes the thermalization. This phenomenon is more obvious as the charge raises. Especially for the case $q = 0.9$, we find the difference of the thermalization curve for different phantom dark energy parameters is most obvious. The effect of the chemical potential on the thermalization is plotted in Figure (3). For (a) in Figure (3), the background recovers to the Vaidya AdS black brane with a chemical potential which was investigated in [21,22,23]. We see that

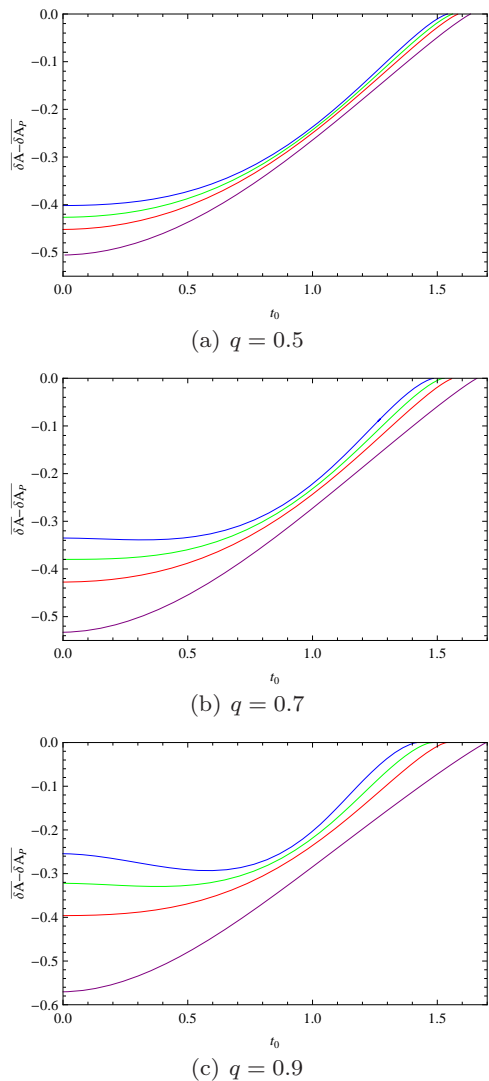


Fig. 2 Thermalization of the renormalized minimal area surface for different phantom dark energy parameters with the same chemical potential at the same boundary separation $l = 2.2$. The purple line, red line, green line, and blue line correspond to $\eta = 1, -1, -2, -3$ respectively.

as the chemical potential increases, the thermalization time enhances. That is, the chemical potential delays the thermalization, which is consistent with that obtained in [21,22,23]. For (b),(c),(d) in Figure (3), we find that as the charge increases, the thermalization time decreases. This effect is not the same as that in (a). Note that for the case $\eta = -1, -2, -3$, the chemical potential is monotonously decreasing as the charge increases. Thus we also can conclude that as the chemical potential increases, the thermalization time raises too. Namely the chemical delays the thermalization always though this seems different for the negative parameters and positive parameters as the charge increases.

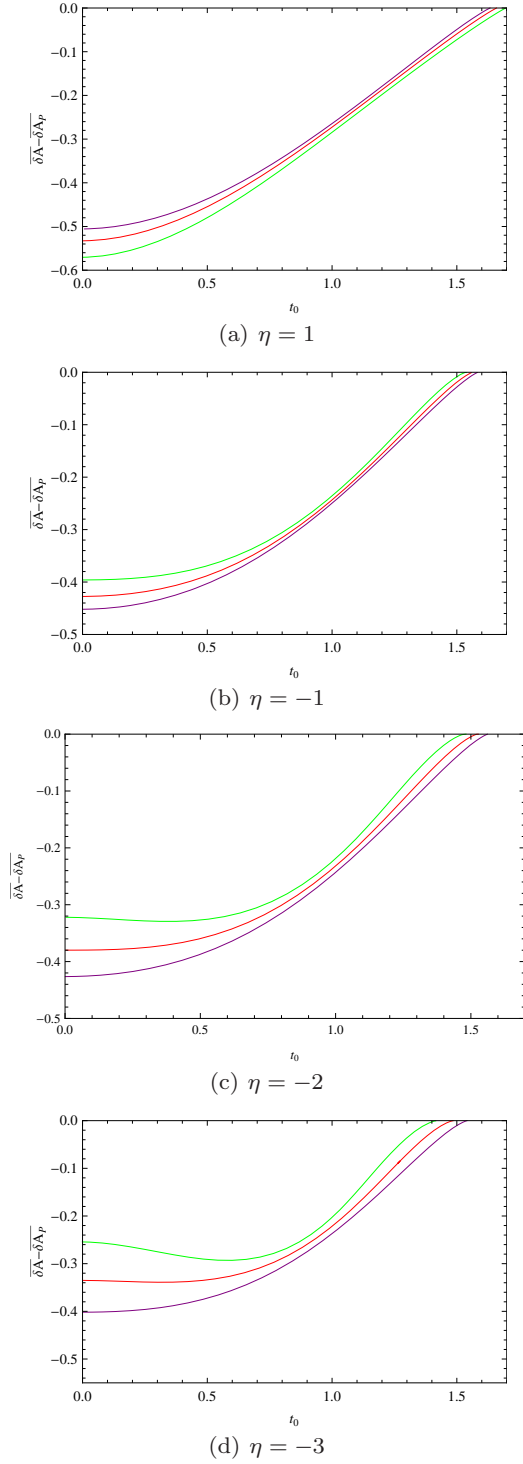


Fig. 3 Thermalization of the renormalized minimal area surface for different chemical potentials with the same phantom dark energy parameter at the same boundary separation $l = 2.2$. The purple line, red line, and green line correspond to 0.5, 0.7, 0.9 respectively.

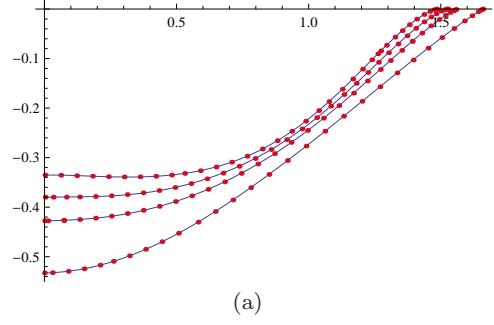


Fig. 4 Comparison of the thermalization process between the numerical curves and fitting functions.

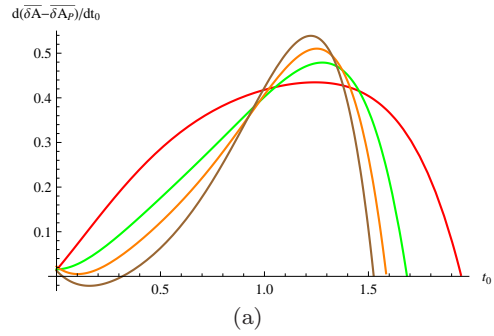


Fig. 5 Thermalization velocity of the renormalized minimal area surface at $q = 0.7$. The red line, green line, orange line, and brown line correspond to $\eta = 1, -1, -2, -3$ respectively.

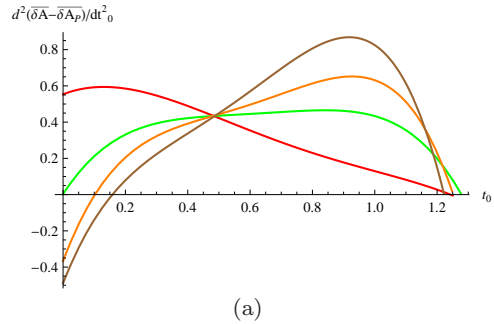


Fig. 6 Thermalization acceleration of the renormalized minimal area surface at $q = 0.7$. The red line, green line, orange line, and brown line correspond to $\eta = 1, -1, -2, -3$ respectively.

In addition, we find the numeric curves for the thermalization process can be fitted as analytical functions with respect to the thermalization time. Thereafter, we mainly focus on the effect of the phantom dark energy parameter on the thermalization. As an example, we consider the case $q = 0.7$. The fitting functions of the thermalization curves for $\eta = 1, -1, -2, -3$ can be ex-

pressed as

$$\left\{ \begin{array}{l} -0.532952 + 0.0142505t_0 + 0.276771t_0^2 + 0.111791t_0^3 \\ \quad - 0.260812t_0^4 + 0.151048t_0^5 - 0.0328631t_0^6 \\ -0.427766 + 0.0156803t_0 + 0.00149207t_0^2 + 0.442568t_0^3 \\ \quad - 0.52845t_0^4 + 0.346392t_0^5 - 0.0937172t_0^6 \\ -0.380358 + 0.0222836t_0 - 0.18342t_0^2 + 0.76406t_0^3 \\ \quad - 0.913827t_0^4 + 0.638737t_0^5 - 0.179835t_0^6 \\ -0.335312 + 0.0126767t_0 - 0.244621t_0^2 + 0.73413t_0^3 \\ \quad - 0.859683t_0^4 + 0.690742t_0^5 - 0.219645t_0^6 \end{array} \right.$$

Figure (4) is the comparison of the numerical curves and fitting function curves. It is obvious that at the order of t_0^6 , the thermalization curves can be described well by the fitting functions. With the analytical functions of the thermalization curves, we can get the thermalization velocity, and thermalization acceleration conveniently. From the thermalization velocity curves in Figure (5), we find the thermalization process is similar for different phantom dark energy parameters, namely at the middle stage of the thermalization process there is a phase transition point which divides the thermalization into an acceleration phase and a deceleration phase. This result is reasonable because the thermalization can not accelerate always in order to approach to an equilibrium state. The phase transition points can also be read off from the null point of the acceleration curves, which are plotted in Figure (6). For the negative phantom dark energy parameter, we find as the parameter decreases, the phase transit decreases. For all the phantom dark energy parameters, we find the initial acceleration of renormalized minimal area surface decreases as the state parameter decreases. Correspondingly, the initial thermalization velocity of minimal area surface decreases gradually. In addition, from Figure (5) and Figure (6) we find the maximum acceleration and maximum velocity increase as the phantom dark energy parameters decrease.

4 Conclusions

We construct a gravitational collapse model which is interpolated between a pure AdS space and a phantom Reissner-Nordstrom AdS black brane. We probe this collapse behavior with the minimal area surface. According to the language of AdS/CFT correspondence, this is dual to probe the thermalization behavior of the quark gluon plasma by the expectation value of Wilson loop in the dual conformal field theory. We focus mainly on the effect of phantom dark energy and chemical potential on the thermalization time. We find for a fixed chemical potential, the smaller the phantom dark

energy parameter is, the easier the plasma thermalizes. And for a fixed dark energy parameter, the larger the chemical potential is, the harder the plasma to thermalize. For the effect of chemical potential on the thermalization time, there are two points should be stressed:

- (22)• From Figure (3), we know that as the charge raises, the thermalization time enhances for the case $\eta = 1$, while it decreases for the case $\eta = -1, -2, -3$. However, in the dual conformal field theory, the quantity which is meaningful physically is the chemical potential not the charge. With the consideration that for $q > 0.5$, the chemical potential raises for $\eta = 1$, while it decreases for $\eta = -1, -2, -3$ as the charge grows. Thus *in the parameter range* which we choose, we can conclude that the chemical potential delays the thermalization for all the phantom dark energy parameters.
- From Figure (1), we know that the chemical potential is not a monotone function with respect to the charge. For $0 < q < 0.49, 0 < q < 0.35, 0 < q < 0.28$, the chemical potential is monotonously increasing as the charge raises for $\eta = -1, -2, -3$ respectively. Thus, if we choose the smaller charge, e.g. $q = 0.2$, we find the chemical potential promotes the thermalization, which is different from the previous result that the chemical potential delays the thermalization. So strictly speaking, the effect of the chemical potential on the thermalization time depends on the dark energy parameters.

Besides our previous investigation, we also obtain the fitting functions of the thermalization curves, and with the functions, we further investigate the thermalization velocity and thermalization acceleration. From the thermalization velocity curves, we know that at the middle stage of the thermalization there is a phase transition point which separates the thermalization into an acceleration phase and a deceleration phase. The phase transition point is found to be shifted for different dark energy parameters. Especially for $\eta = -1, -2, -3$, we find the phase transit decreases as the phantom dark energy parameter decreases. Both the maximum acceleration and maximum velocity are found to be increased as the dark energy parameters decrease. Though our study in this part is not so strict as that in [61,62], where the whole thermalization was divided into four processes and the analytical function for each process was given strictly, our investigation can provide another sight to understand the thermalization process.

Acknowledgements This work is supported by the National Natural Science Foundation of China (Grant No. 11405016 and No. 11205226).

References

1. J. M. Maldacena, Adv. Theor. Math. Phys. **2**, 231 (1998)
2. J. Sonner, A. G. Green, Phys. Rev. Lett. **109**, 091601 (2012)
3. W. J. Li, Y. Tian, H. Zhang, JHEP **07**, 030(2013)
4. K. Murata, S. Kinoshita, N. Tanahashi, JHEP **1007**, 050 (2010)
5. Y. Ling, C. Niu, J. Wu, Z. Xian, H. Zhang, Phys. Rev. Lett. **113**, 091602 (2014)
6. S. A. Hartnoll, C. P. Herzog, G. T. Horowitz, Phys. Rev. Lett. **101**, 031601 (2008)
7. R. G. Cai, R. Q. Yang, Phys. Rev. D **90**, 081901 (2014)
8. J. Mas, JHEP **0603**, 016 (2006)
9. D. Garfinkle, L. A. Pando Zayas, Phys. Rev. D **84**, 066006 (2011)
10. D. Garfinkle, L. A. Pando Zayas, D. Reichmann, JHEP **1202**, 119 (2012)
11. A. Allais, E. Tonni, JHEP **1201**, 102 (2012)
12. S. R. Das, J. Phys. Conf. Ser. **343**, 012027 (2012)
13. D. Steineder, S. A. Stricker and A. Vuorinen, probing the pattern of holographic thermalization with photons, arXiv:1304.3404 [hep-ph].
14. B. Wu, JHEP **1210**, 133 (2012)
15. X. Gao, A. M. Garcia-Garcia, H. B. Zeng, H. Q. Zhang, Lack of thermalization in holographic superconductivity, arXiv:1212.1049 [hep-th].
16. A. Buchel, L. Lehner, R. C. Myers, A. van Niekerk, JHEP **1305**, 067 (2013)
17. V. Keranen, E. Keski-Vakkuri, L. Thorlacius, Phys. Rev. D **85**, 026005 (2012)
18. V. Balasubramanian *et al.*, Phys. Rev. Lett. **106**, 191601 (2011)
19. V. Balasubramanian *et al.*, Phys. Rev. D **84**, 026010 (2011)
20. R. Baier, A. H. Mueller, D. Schiff, D. Son, Phys. Lett. B **502**, 51 (2001)
21. D. Galante, M. Schvellinger, JHEP **1207**, 096 (2012)
22. E. Caceres, A. Kundu, JHEP **1209**, 055 (2012)
23. E. Caceres, A. Kundu, D. L. Yang, Jet Quenching and Holographic Thermalization with a Chemical Potential, arXiv:1212.5728 [hep-th].
24. X. X. Zeng, W. B. Liu, Phys. Lett. B **726**, 481(2013)
25. X. X. Zeng, X. M. Liu, W. B. Liu, JHEP **03**, 031(2014)
26. W. H. Baron and M. Schvellinger, JHEP **08**, 035(2013)
27. Y. Z. Li, S. F. Wu, G. H. Yang, Phys. Rev. D **88**, 086006 (2013)
28. W. Baron, D. Galante, M. Schvellinger, JHEP **1303**, 070 (2013)
29. I. Arefeva, A. Bagrov, A. S. Koshelev, JHEP **07**, 170(2013)
30. V. E. Hubeny, M. Rangamani, E. Tonni, JHEP **05**, 136 (2013)
31. I. Y. Arefeva, I. V. Volovich, On Holographic Thermalization and Dethermalization of Quark-Gluon Plasma, arXiv:1211.6041 [hep-th].
32. V. Balasubramanian *et al.*, JHEP **04**, 069,(2013)
33. V. Balasubramanian *et al.*, JHEP **10**, 082,(2013)
34. V. Balasubramanian *et al.*, Phys. Rev. Lett. **111**, 231602 (2013)
35. V. Balasubramanian *et al.*, Phys. Rev. Lett. **113**, 071601 (2014)
36. P. Fonda *et al.*, JHEP **1408**, 051(2014)
37. V. Cardoso *et al.*, JHEP **04**, 183(2014)
38. V. E. Hubeny, H. Maxfield, JHEP **03**, 097 (2014)
39. X. X. Zeng, X. M. Liu, and W. Liu, Holographic thermalization in noncommutative geometry, arXiv:1407.5262[hep-th].
40. A. Giordano, N. E. Grandi, G. A. Silva, Holographic thermalization of charged operators, arXiv:1412.7953[hep-th].
41. S. J. Zhang, B. Wang, E. Abdalla, E. Papantonopoulos, Holographic Thermalization in Gauss-Bonnet Gravity with de Sitter Boundary, arXiv:1412.7073[hep-th].
42. G. Camilo, B. Cuadros-Melgar, E. Abdalla, Holographic thermalization with a chemical potential from Born-Infeld electrodynamics, arXiv:1412.3878[hep-th].
43. A. Buchel, R. C. Myers, A. van Niekerk, Nonlocal probes of thermalization in holographic quenches with spectral methods, arXiv:1410.6201[hep-th].
44. X. X. Zeng, D. Y. Chen, L. F. Li, Holographic thermalization and gravitational collapse in the spacetime dominated by quintessence dark energy, arXiv:1408.6632[hep-th].
45. E. Komatsu *et al.*, Astrophys. J. Suppl. **192**, 18 (2011)
- S. Perlmutter *et al.*, Ap. J. **517**, 565 (1999);
- A. G. Riess *et al.*, Ap. J. **560**, 49 (2001);
- J. P. Blakeslee *et al.*, Ap. J. **589**, 693 (2003)
46. S. M. Carroll, M. Hoffman, M. Trodden, Phys. Rev. D **68**, 023509 (2003);
- P. Singh, M. Sami, N. Dadhich, Phys. Rev. D **68**, 023522 (2003)
47. S. Hannestad, Int. J. Mod. Phys. A **21**, 1938 (2006)
48. J. Dunkley *et al.*, Astrophys. J. Suppl. Ser. **180**, 306 (2009)
49. G. W. Gibbons, D.A. Rasheed, Nucl. Phys. **B476**, 515 (1996)
50. C. J. Gao, S. N. Zhang, Phantom Black Holes, arXiv:hep-th/0604114.
51. G. Clément, J.C. Fabris and M.E. Rodrigues, Phys. Rev. D **79**, 064021 (2009)
52. M. Azreg-Aïnou, G. Clément, J.C. Fabris and M.E. Rodrigues, Phys. Rev. D **83**, 124001 (2011)
53. M. E. Rodrigues and Z. A. A. Oporto, Phys. Rev. D **85**, 104022 (2012)
54. M. Azreg-Aïnou, Phys. Rev. D **87**, 024012 (2013)
55. G. N. Gyulchev, I. Zh. Stefanov, Phys. Rev. D **87**, 063005 (2013)
56. D. F. Jardim, M. E. Rodrigues, M. J. S. Houndjo, Eur. Phys. J. Plus **127**, 123 (2012)
57. A. Chamblin, R. Emparan, C. V. Johnson, R. C. Myers, Phys. Rev. D **60**, 064018 (1999).
58. J. M. Maldacena, Phys. Rev. Lett. **80**, 4859 (1998)
59. R. M. Wald, General Relativity, University of Chicago Press, 1984.
60. Y. Ling, C. Niu, J. P. Wu, Z. Y. Xian, JHEP **11**, 006(2013)
61. H. Liu, S. J. Suh, Phys. Rev. Lett. **112**, 011601 (2014)
62. H. Liu, S. J. Suh, Phys. Rev. D **89**, 066012 (2014)